Proc. Natl. Acad. Sci. USA
Vol. 93, pp. 13870–13875, November 1996
Genetics

The mouse *Pax2*^{1Neu} mutation is identical to a human *PAX2* mutation in a family with renal-coloboma syndrome and results in developmental defects of the brain, ear, eye, and kidney

JACK FAVOR*†, RODICA SANDULACHE*, ANGELIKA NEUHÄUSER-KLAUS*, WALTER PRETSCH*, BIMAL CHATTERJEE*, ELFRIEDE SENFT‡, WOLFGANG WURST*, VÉRONIQUE BLANQUET*, PATRICIA GRIMES§, RALF SPÖRLE*, AND KLAUS SCHUGHART*

*GSF–National Research Center for Environment and Health, Institute of Mammalian Genetics, and ‡Institute of Pathology, Neuherberg, Ingolstädter Landstrasse 1, D-85764 Oberschleissheim, Germany; and §Department of Ophthalmology, The School of Medicine and Scheie Eye Institute, University of Pennsylvania, Philadelphia, PA 19104-6075

Communicated by Mary F. Lyon, Medical Research Council, Oxfordshire, United Kingdom, September 10, 1996 (received for review July 19, 1996)

ABSTRACT **We describe a new mouse frameshift mutation (*Pax2*^{1Neu}) with a 1-bp insertion in the *Pax2* gene. This mutation is identical to a previously described mutation in a human family with renal-coloboma syndrome [Sanyanusin, P., McNoe, L. A., Sullivan, M. J., Weaver, R. G. & Eccles, M. R. (1995) *Hum. Mol. Genet.* 4, 2183–2184]. Heterozygous mutant mice exhibit defects in the kidney, the optic nerve, and retinal layer of the eye, and in homozygous mutant embryos, development of the optic nerve, metanephric kidney, and ventral regions of the inner ear is severely affected. In addition, we observe a deletion of the cerebellum and the posterior mesencephalon in homozygous mutant embryos demonstrating that, in contrast to mutations in *Pax5*, which is also expressed early in the mid-hindbrain region, loss of *Pax2* gene function alone results in the early loss of the mid-hindbrain region. The mid-hindbrain phenotype is similar to *Wnt1* and *En1* mutant phenotypes, suggesting the conservation of gene regulatory networks between vertebrates and *Drosophila*.**

The recovery and characterization of mutations in the mouse have been important for the understanding of gene function in mammals and they have served as models for human genetic disease. The *Pax* gene family is especially interesting. *Pax* genes are characterized by a conserved sequence element, the paired box, that was originally described in the *Drosophila* pair-rule gene named "paired." Nine members of the *Pax* gene family in mammals are known, and by the analysis of mouse mutations, *Pax* genes have been shown to play an essential role in early mammalian development (1–3). The mouse mutations *undulated*, *Splotch*, and *Small eye* (*Pax1*, *Pax3*, and *Pax6*, respectively) result in abnormal development of the vertebral skeleton, thymus, central and peripheral nervous system, limb muscles, nose, and eye (for review, see refs. 1 and 3). In humans, mutations of the *PAX3* gene were found in patients with Waardenburg syndrome type 1, and *PAX6* gene alterations were identified in patients with aniridia or Peters anomaly (for review, see refs. 1 and 3).

Two human families with renal-coloboma syndrome have been described with frameshift mutations in the *PAX2* gene. A deletion of a single nucleotide in exon 5 results in a predicted truncated protein that contains the paired domain and the octapeptide but lacks the (partial) homeodomain sequence (4). Patients exhibited bilateral optic nerve colobomas and various degrees of kidney abnormalities (ranging from progressive renal failure to no detectable defects). In a second family, a single nucleotide insertion was observed in the 5′ region of the *PAX2* gene resulting in a frameshift mutation and a stop codon 26 aa downstream (5). The mutant gene is predicted to code for a nonfunctional protein lacking almost the entire paired domain and the complete homeodomain. The two affected siblings from this family exhibit optic nerve colobomas as well as severe or mild chronic renal failure.

In mouse and zebrafish embryos, expression of the *Pax2* gene was described in the central nervous system, eye, ear, and nephrogenic ducts and mesenchymes (6–9). In the central nervous system, *Pax2* expression is found in the developing mid-hindbrain junction and in subregions of the ventricular and mantle layers of the developing spinal cord (6, 8, 9). *Pax2* expression in the mid-hindbrain region precedes the onset of *En1*, *En2*, *Wnt1*, and *Pax5* gene expression and it was suggested that *Pax2* may be required for the activation and/or maintainance of these genes (9–11). In the developing eye, *Pax2* is first expressed in distal regions of the optic vesicle, then in ventral regions of the optic cup and stalk, and later, in the optic disc and along the outgrowing optic nerve (6). When the neural epithelium of the retina differentiates into the different nuclear layers, *Pax2* expression can be found in the neuroblastic layer in a thin layer of cells facing the vitreous chamber (6). Expression in the developing ear was described in the otic vesicle and, at later stages, in the developing ventral region of the inner ear (6). In the developing intermediate mesoderm of the mouse, *Pax2* expression was observed in pro- and mesonephric tubules, the developing Wolffian and Müllerian duct, the developing ureter, and in mesenchymal condensations that form around the developing collecting ducts of the metanephric mesenchyme (7, 12).

Two mouse strains with mutations in the *Pax2* gene have been described. The *Krd* strain carries a large chromosomal deletion [≈7 centimorgans (cM)] of the distal region of chromosome 19 including the *Pax2* locus (13). Heterozygous *Krd* mice develop retinal abnormalities (abnormal electroretinograms and reduced cell numbers in all nuclear layers of the retina) and a high incidence of kidney defects (hypoplastic and cystic kidneys). Expressivity of both defects is variable among individual heterozygous animals (13) and homozygotes are lethal in the preimplantation stage. Torres *et al.* (12) have generated a *Pax2* knockout mutation in the mouse. They describe severe abnormalities in development of the meso- and metanephric mesenchymes in homozygous embryos that result in the absence of genital tracts and metanephric kidneys. Heterozygous mutants frequently showed reductions in kidney size. Other aspects of the heterozygous or homozygous mutant phenotype have not been described.

The publication costs of this article were defrayed in part by page charge payment. This article must therefore be hereby marked "*advertisement*" in accordance with 18 U.S.C. §1734 solely to indicate this fact.

Abbreviations: p.c., postcoitus; TS, Theiler stage.

Data deposition: The sequence reported in this paper has been deposited in the GenBank data base (accession no. Y07617 for the *Pax2* sequence).

†To whom reprint requests should be addressed.

Herein, we report a new mutant *Pax2* allele (*Pax2*^{1Neu}) in the mouse with the identical 1-bp insert frameshift mutation as observed in a human family with renal-coloboma syndrome. *Pax2*^{1Neu} heterozygotes exhibit defects in the neural retina and kidneys, and homozygous mutant embryos show malformations of the nephrogenic mesenchyme. In addition to previous reports, we observed abnormal development of the mid-hindbrain region, the optic nerve, and ventral regions of the inner ear in homozygous *Pax2* mutant embryos.

MATERIALS AND METHODS

Mice. All mutant and inbred strains of mice employed were obtained from breeding colonies maintained in Neuherberg.

Ophthalmologic Examination. The eye phenotype of mice in the mutant breeding colony as well as in the intraspecific backcross was determined at weaning (3 weeks). Dilation of the pupils was achieved with a drop of 1% atropine applied to the eyes at least 10 min before examination. For each animal, both eyes were examined by slit lamp biomicroscopy (Zeiss SLM30) at ×48 magnification.

Genomic Mapping. Genomic DNA was extracted from livers of offspring from the cross (C3H × C57BL/6 K289/+) × C57BL/6. Segregation analysis of the K289 mutation was carried out with 42 Mit-microsatellite markers distributed among the 19 mouse autosomes that are informative for the cross between strains C3H or 102 and C57BL/6. All PCR amplifications were carried out according to the manufacturer's specifications (Boehringer Master Mix *Taq* polymerase) with the following amplification program: a 4-min 94°C denaturation followed by 30 cycles (1-min 94°C denaturation; 1-min 55°C annealing; 2-min 72°C extension) and a final extension of 5 min at 72°C. Amplification products were electrophoretically separated in 3% agarose gels and visualized by ethidium bromide staining.

***In Situ* Hybridization and Histology.** *In situ* hybridization and histological analysis of embryos was performed as described (14). Staging of embryos was done according to Kaufman (15): Theiler stage (TS) 15, day ≈9.5 postcoitus (p.c.); TS17, day ≈10.5 p.c.; TS19, day ≈11.5 p.c.; TS21, day ≈12.5 p.c.; TS22, day ≈13.5 p.c.; TS23, day ≈14.5 p.c.

Eye Histology. Adult (3–6 months of age) animals were sacrificed by cervical dislocation and eyes were fixed immediately in 4% paraformaldehyde, embedded in Historesin (Leica Instruments, Heidelberg, Germany), serially sectioned at 3.5 μm, and stained with toluidine blue for light microscopic examination. All animals used were from crosses of the K289 mutation to (102 × C3H)F_1 hybrids. Since in these crosses the *rd* mutation is segregating, all adult mice demonstrating reduction of the photoreceptor layer to a single row of nuclei throughout the retina were assumed to be *rd*/*rd* homozygotes (16) and were excluded from the histological evaluations.

PCR, Reverse Transcription-Coupled PCR, and Analysis of *Pax2* Sequences. Wild-type strain C3H or affected TS21 embryos (12.5 day p.c.) from *inter se* crosses were prepared in PBS. Brain and spinal cord regions were isolated and used for RNA; the remaining tissue was used for DNA extraction. RNA was prepared using the RNeasy Kit (Qiagen, Chatsworth, CA). First-strand cDNA synthesis was performed with a gene-specific primer and SuperscriptII (Boehringer) as recommended by the supplier. DNA was prepared according to standard procedures (17). Amplification of *Pax2* cDNA fragments was achieved by using three different overlapping primer sets (the corresponding nucleotide positions are given in parentheses): 1, 5′-TCCTGAAGTTGAGTTTGAGAGGC-3′ (nt 257–279)/5′-TTTCCTCTTCTCACCGTTGG-3′ (nt 908–927); 2, 5′-TGTTTCCAGCGCCTCTAACGAC-3′ (nt 840–861)/5′-ACTGGACTTGACTTCATCAAGCC-3′ (nt 1217–1239); 3, 5′-ATGTCTTCCAGGCATCAGAGC-3′ (nt 1145–1165)/5′-TGCCTGAAGCTTGATGTGGTC-3′ (nt 1583–1603). The resulting PCR products were HPLC purified, reamplified, and sequenced with a *Taq* Dye-Deoxy terminator cycle sequencing kit by SequiServe (Vaterstetten, Germany).

Genotyping of Embryos. Presumed homozygous *Pax2*^{1Neu} embryos were identified by phenotype (mid-hindbrain deletion). The genotype was confirmed by PCR amplification of genomic DNA and sequencing as described above. The primers with the corresponding nucleotide positions used were 5′-GGCACGGGGGTGTGAAC-3′ (nt 368–384) and 5′-TGACACAGCCATGGCTGACC-3′ (nt 498–517).

RESULTS

Linkage Analysis and Mutation Characterization. The spontaneous mutation K289 was originally recovered in a (102 × C3H)F_1 hybrid mouse as a heterozygote expressing abnormal blood vessel formations in the fundus that extended into the vitreous chamber as well as posterior capsular opacities. Histological analysis confirmed these observations (see below). Segregation analysis indicated K289 to be autosomal dominant and the mutation was subsequently bred to strain 102 (15 generations) and then crossed to (102 × C3H)F_1 hybrid mice (6 generations).

Strain 102 has been shown to be a recombinant inbred strain between strains 101 and C3H and fixed at approximately 70% of the loci studied for the allele carried by strain C3H (18). Of possible significance is the retinal degeneration (*rd*) locus in which strains 102 and C57BL/6 are +/+ and strain C3H is *rd*/*rd*. In clinical examinations, we observed no phenotypic differences of K289/+ heterozygotes maintained on strain 102 or (102 × C3H)F_1 or in the outcross and backcross to strain C57BL/6.

Linkage analyses were undertaken via a genome wide microsatellite screen and the mutation was localized between D19Mit11 and D19Mit91 (Fig. 1 *A* and *B*), which is close to the reported chromosomal position of *Pax2* (2, 13). Heterozygotes were bred *inter se*, and inspection of embryos between TS17 and TS23 (day 10.5–14.5 p.c.) revealed offspring expressing a deletion of the mid-hindbrain region (see below). RNA from brains of presumed homozygous embryos was extracted, *Pax2* mRNA was amplified, and sequence analysis revealed an insertion of a single guanosine (Fig. 1*C*). The mutation was confirmed by sequencing from genomic DNA. We hereby

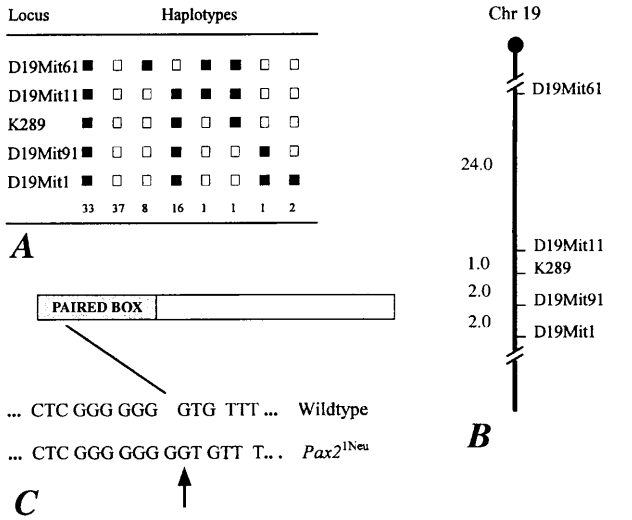

FIG. 1. Chromosomal mapping of the K289 mutation to the distal region of chromosome 19 and sequence analysis of the mutant *Pax2*^{1Neu} allele. (*A*) Distribution of haplotypes in backcross animals. Solid boxes, C3H allele; open boxes, C57BL/6 allele. (*B*) Schematic presentation of distal chromosome 19. (*C*) Partial sequence of the wild-type and mutant *Pax2*^{1Neu} alleles.

designate this mutant allele *Pax2*^{1Neu}. Exactly the same mutation has been described in the human *PAX2* gene in a family with autosomal dominant renal-coloboma syndrome (5). The mouse and human mutations are spontaneous in origin, occur at a site of 7 guanosine repeats (positions 391–397), and may be due to replication slippage.

The frameshift mutation results in a premature stop codon. The predicted mutant peptide contains 51 aa of which the first 24 aa are identical to those of the wild-type protein. In the remaining 27 aa of the mutant peptide, there was only 1 aa match with the wild-type protein. In all other regions, our sequencing data showed no differences between the mutant and the wild-type *Pax2* genes. However, there were several differences observed between our wild-type *Pax2* sequence with the published mouse *Pax2* sequence (7). In the paired domain, six nucleotide differences were noted at positions 668, 669, 690, 691, 699, and 700. Only one (position 690) was different from the published human *PAX2* sequence (19). All six involved codons code for the identical amino acid in the human sequence and in the presently described sequence. There were two nucleotide differences to the published mouse *Pax2* sequence at positions 1350 and 1354 that were also identical to the published human *PAX2* sequence. At the positions 1546 and 1547, two nucleotide substitutions were observed and a single codon insert was identified between positions 1530 and 1531. In these cases, the published mouse and human sequences were concordant. In the 5′ region of the *Pax2* coding sequence, we observed a single codon insert between the positions 367 and 368 that was identical to the human *PAX2* sequence. Based on the human genomic DNA sequence (4), this position corresponds to the 5′ end of exon 2. There is a CAGCAG trinucleotide repeat and the AG dinucleotide serves as the donor acceptor site. To confirm our observations, three independently cloned *Pax2* cDNAs were sequenced, two of which were identical to the published mouse *Pax2* sequence (lacking the additional codon). The third clone contained the codon insert that was observed in the human *PAX2* sequence. These results suggest that there is alternative splicing involving the AG dinucleotides in the CAGCAG trinucleotide repeat.

Our sequence data are based upon cDNA or genomic DNA from a C3H background, whereas the published mouse *Pax2* sequence is from strain NMRI. To determine if strain differences could explain these discrepancies, we also sequenced the *Pax2* gene from strains NMRI and C57BL/6 maintained in Neuherberg. There were no differences in the *Pax2* sequence for the strains that we have tested. We cannot exclude substrain differences as a possible explanation for the discrepancies observed.

Phenotype of Heterozygous Carriers. The adult heterozygote *Pax2*^{1Neu} eye was characterized by optic disc dysplasia, abnormalities of the entering retinal blood vessels, and thinning of the nerve fiber and ganglion cell layers of the retina. The heterozygous eye illustrated in Fig. 2 had an abnormally broad and cup-shaped optic disc from which blood vessels projected into the vitreous cavity (Fig. 2*B*). Adjacent to the disc, all neural layers of the retina were drastically thinned in comparison to the normal eye (Fig. 2 *A* and *B*). Ganglion cells and their axons in the nerve fiber layer, prominent in this region of the normal retina, were very sparse in the mutant eye. In more peripheral regions of the retina, the photoreceptor layer of the heterozygote (Fig. 2*D*) was comparable in thickness and structure to that in the normal eye (Fig. 2*C*) but, as also observed in *Krd* mice (13), all inner retinal layers were notably thinned. Preretinal vessels (Fig. 2*D*), never seen in the normal eye, were distributed all along the internal surface of the mutant retina. Preretinal vessels were a variable feature of the phenotype; other heterozygous eyes had normally located intraretinal blood vessels despite the structural abnormalities at the optic disc. Although we have eliminated from our analyses all animals expressing the typical *rd*/*rd* phenotype, caution still must be exercised in conclusions of the general retinal pathology of *Pax2*^{1Neu}/+ animals. Nevertheless, our most important finding, the severe abnormality of the optic disc region, would not be complicated by the segregation of *rd* in our crosses. This ocular defect is also consistent with the clinically observed phenotype associated with *PAX2* mutations in humans, characterized by abnormalities of the optic nerve head including large discs with irregular cups, thin neuroretinal rims, anomalous vascular pattern, and defects in the peripapillary pigmented epithelium and choroid (4, 5, 20). We have not yet systematically examined heterozygotes for other pathological defects. However, while preparing organs from the intraspecific backcross mice for genomic DNA extractions, 3 of 50 *Pax2*^{1Neu}/+ mice were observed to have only one kidney and numerous heterozygotes were observed with small and/or cystic kidneys.

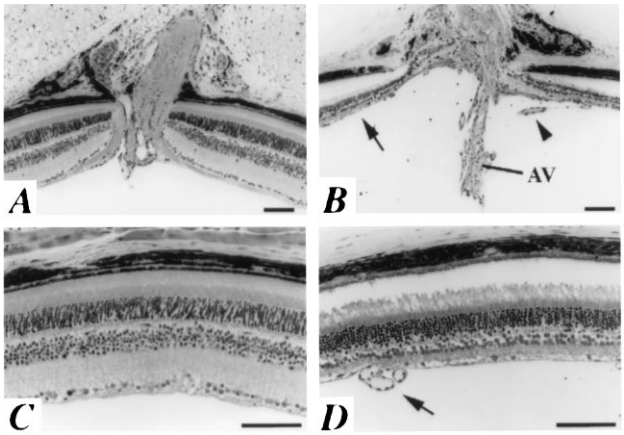

FIG. 2. Eye defects in heterozygous *Pax2*^{1Neu} mice. Retinal morphology of adult (3–6 months of age) wild-type (*A* and *C*) and heterozygous (*B* and *D*) mice. In comparison to the normal eye (*A*), note the broad and cup-shaped optic disc in the heterozygote (*B*) and pronounced thinning of all neural layers of the adjacent retina (arrow). An arterial vessel (AV) projects into the vitreous; a small branch vessel (arrowhead) arches to the surface of the retina. Beyond the immediate region of the optic disc, the inner retinal layers of the heterozygous eye (*D*) are still markedly thinned, but the photoreceptor layer is similar in thickness to that in the normal eye (*C*). Preretinal vessels (arrow) are visible all along the inner surface of the mutant retina (*D*). (Bars = 100 μm.)

Phenotype of Homozygous Embryos: Mid-Hindbrain. At TS21 (12.5 days p.c.), the mesencephalon, metencephalon, and myelencephalon were readily distinguishable (Fig. 3*A*) in wild-type embryos, whereas in homozygous embryos a deletion of the mid-hindbrain region was clearly evident (Fig. 3*B*). At TS23 (day 14.5 p.c.) in wild-type embryos, the anlagen of the cerebellum has formed from the mid-hindbrain region, and the midbrain starts to differentiate into inferior and superior colliculi (Fig. 3*C*). Histological sections of TS23 *Pax2*^{1Neu} mutant brains showed a deletion of the cerebellum and posterior mesencephalon (Fig. 3*D*). The choroid plexus, normally attached to the cerebellum, was fused to the superior colliculi in mutant embryos (Fig. 3*D*). At TS15, a shortening of the presumptive brain region in whole mounts of homozygous mutant embryos was visible and suggested a deletion of the mid-hindbrain region (Fig. 3*F*). At this stage, *En2* is expressed in a broad band of cells in the mid-hindbrain region of wild-type embryos (Fig. 3*E*, arrowheads) and can thus be used as an early marker for the presence or absence of the mid-hindbrain region (for review, see ref. 21). Analysis of *Pax2* mutant embryos revealed that the *En2* expression domain was almost completely absent (Fig. 3*F*), with the exception of a small region in the dorsal neural tube, which is consistent with a deletion of the mid-hindbrain region already at early stages

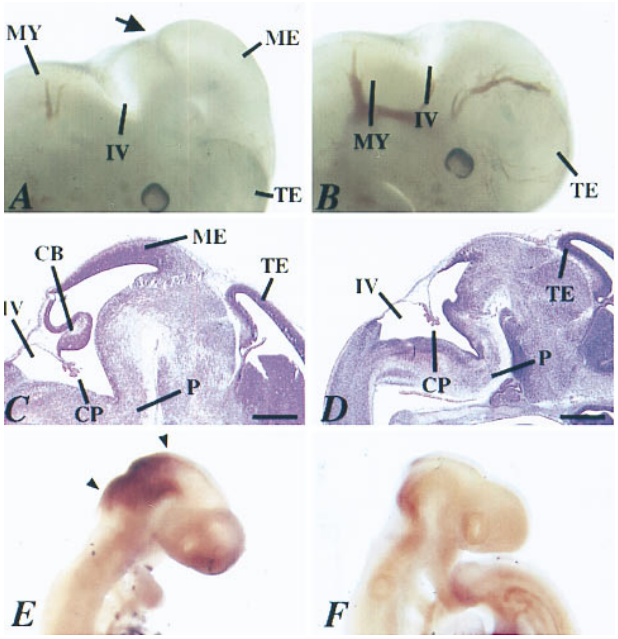

FIG. 3. Defects in development of the mid-hindbrain region in *Pax2*^{1Neu} mutant embryos. Wild-type (*A, C,* and *E*) and mutant (*B, D,* and *F*) embryos. (*A* and *B*) Overview of head region of TS21 embryos. The mid-hindbrain junction (isthmus) is clearly visible in wild-type (*A*) (arrow) but absent in mutant (*B*) embryos. (*C* and *D*) Sagittal sections through head regions of TS23 embryos. The anlagen of the cerebellum and most parts of the mesencephalon are missing in mutant embryos whereas the pons appears to be unaffected (*D*). (*E* and *F*) TS15 whole-mount embryos hybridized with an *En2*-specific RNA probe. In wild-type, *En2* is expressed in a broad band across the mid-hindbrain region (*E*) (arrowheads). In mutants (*F*), *En2* expression was greatly reduced to a small region in the dorsal neural tube. IV, fourth ventricle; CB, cerebellum; CP, choroid plexus; ME, mesencephalon; MY, myelencephalon; P, pons; TE, telencephalon. (*C* and *D*, bars = 500 μm.)

of brain development. At stage TS15, we also noted a delay of neural tube closure in the mid-hindbrain region in homozygous mutant embryos. In total, we observed brain defects in 26% (20 of 75) of the embryos from heterozygous *inter se* crosses: 21% showed mid-hindbrain deletions; 5% exhibited an exencephaly.

Phenotype of Homozygous Embryos: Inner Ear. At TS23 (14.5 days p.c.), different portions of the inner ear can be distinguished. The endolymphatic duct and vestibula develop from dorsal and the cochlea develops from ventral regions of the otic vesicle. The vestibular portion forms the three semicircular canals and ampullae; the ventral portion of the otocyst coils and forms the cochlea (22). Vestibula and cochlea are connected via a chamber that, at this stage, begins to divide into utriculus and sacculus. The vestibular and cochlear portions are each associated with a distinct part of ganglion VIII. At TS23, semicircular canals were present in both wild-type and *Pax2*^{1Neu} mutant embryos (data not shown). In contrast, the anlagen of the cochlea could not be seen in homozygous mutants (Fig. 4*B*). A distinct formation of the sacculus and, in some cases, utriculus and ampullae of the semicircular canals could not be observed. Instead, an abnormally enlarged chamber was visible ventral to the semicircular canals (Fig. 4*B*, asterisk). This chamber continued dorsally into the enlarged endolymphatic duct. Within the anlagen of ganglion VIII, the presumptive cochlear portions (spiral ganglion) exhibited massive cell death (data not shown). The prominent necrosis and the presence of an enlarged ventral chamber suggest that the cochlea, and possibly other ventral portions of the inner ear, do not properly differentiate in *Pax2* homozygous embryos.

Phenotype of Homozygous Embryos: Eye. During embryonic development of the vertebrate eye, neural and retinal layers develop from a ventral extension of the diencephalon, the optic vesicle. The optic vesicle grows laterally, abuts the surface ectoderm, initiates the final steps in lens induction and then invaginates to form the distal optic cup and proximal optic stalk. The invagination occurs at the distal and ventral sides of the optic vesicle, leaving a ventral fissure in the optic cup and distal optic stalk (22). During axogenesis, the optic nerve exits the optic cup through the ventral fissure and continues into the ventral fissure of the distal stalk and along its ventral wall into the diencephalon (23, 24). In TS23 (14.5 days p.c.) wild-type embryos, the lumen of the distal stalk is narrowed to a vestigial slit, with a flattened shape, and axon fascicles run along the ventral wall (Fig. 4*C*). In homozygous *Pax2*^{1Neu} mutant embryos, however, the distal stalk exhibited a circular shape and the optic nerve contained much less axon fibers. Many fibers were found inside the stalk and, in addition, isolated axon fascicles were present within the ventral, lateral, or dorsal wall (Fig. 4*D*). In more proximal regions, the optic stalk in wild-type embryos still maintained an inner lumen at this stage, and the optic nerve contained prominent axon fascicles arranged in a crescent along the ventral and lateral stalk regions (Fig. 4*E*). In mutant embryos, the inner lumen of the stalk was absent and most fibers were located in the posterior wall of the stalk (Fig. 4*F*). Pigment cells in the distal stalk were not confined to the dorsal-most regions, as seen in wild-type, but were organized in an irregular pattern in the mutant (data not shown). These results suggest that guidance of the optic nerve axons along the optic stalk and/or optic fissure is severely impaired in mutant embryos.

Phenotype of Homozygous Embryos: Kidney. Both the genital tracts and kidneys are generated by derivatives of the intermediate mesoderm. The ducts in the mesonephric mesenchyme form the genital tracts, and in mammals, the definitive kidney develops from the metanephrogenic blastema that requires interactions with the invading ureteric bud. *Pax2* gene expression has been described in both the mesonephric and metanephric ducts and mesenchymes (7, 8). Development of the metanephric kidney starts at about TS22 (13.5 days p.c.) in the mouse embryo, when the ureteric bud grows out from the caudal part of the Wolffian duct and contacts the metanephrogenic blastema. Subsequently, the ureteric bud branches and induces further differentiation of the metanephric mesenchyme. At the tips of the outgrowing ureter buds, the mesenchyme condenses and a secondary epithelium is induced that will give rise to glomeruli and distal and proximal tubules (22). At TS23, tissue sections from wild-type embryos showed development of adrenal gland, gonads, and kidney (Fig. 4*G*) and formation of many tubules in the metanephric kidney. In mutant embryos, adrenal and gonad were present, but only a small anlagen of the presumptive metanephrogenic blastema was detectable (Fig. 4*H*, arrow). The formation of tubules could not be seen in this mesenchyme.

DISCUSSION

We presently report a frameshift mutation within the *Pax2* gene of the mouse that is an exact model of a previously reported human *PAX2* mutation (5). Three mouse *Pax2* mutations have now been identified; *Pax2*^{1Neu}, the *Krd* multilocus deletion (13) and the *Pax2* knockout mutation (12). Two human *PAX2* mutations have been characterized (4, 5). For all five mutations, heterozygous carriers express eye and kidney abnormalities, although there appears to be variability in expressivity and/or reduced penetrance. A detailed characterization of the effects of *Pax2* mutations in heterozygotes is most relevant since human *PAX2* mutations would be expected to occur almost exclusively in heterozygous carriers. We are now able to identify mutation carriers with closely linked

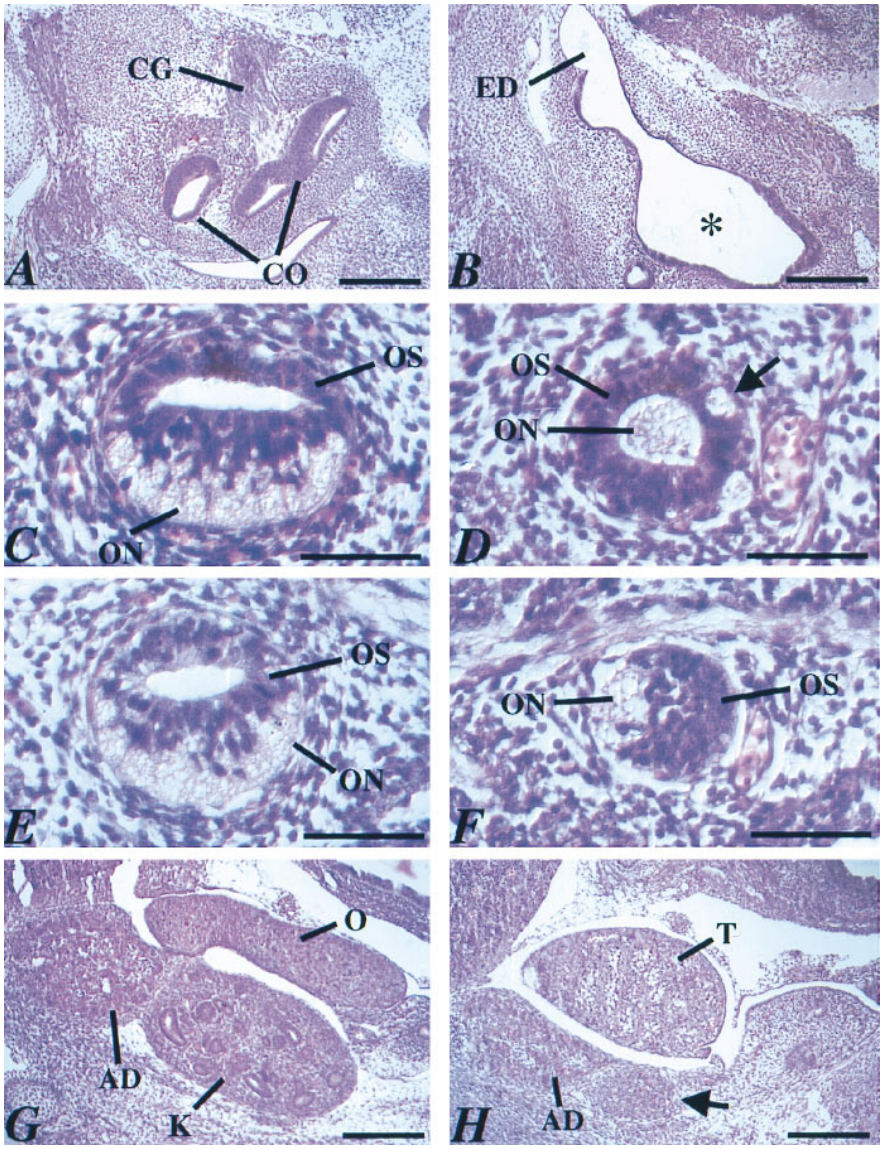

FIG. 4. Defects in development of the inner ear, eye, and nephrogenic mesenchyme in *Pax2*^{1Neu} mutant embryos. Tissue sections from wild-type (*A*, *C*, *E*, and *G*) and mutant (*B*, *D*, *F*, and *H*) TS23 embryos. The inner ear in wild-type embryos showed development of the cochlea and its associated ganglion (*A*). In *Pax2* mutant embryos, formation of a distinct cochlea anlagen could not be found (*B*). Instead, a large chamber was observed that continued into an enlarged endolymphatic duct (*B*) (asterisk). Cross sections through the optic nerve of wild-type (*C* and *E*) and homozygous mutant (*D* and *F*) embryos. In mutant embryos, axon fibers were found inside the optic stalk (*D*) and single isolated axon fascicles could be observed in the ventral, lateral, or dorsal wall of the optic stalk (*D*) (arrow). In more proximal optic stalk regions of homozygous embryos, most axon fibers were seen in the posterior region of the optic stalk (*F*). (*G* and *H*) Sections through urogenital tract of TS23 embryos. In mutant embryos, adrenal and gonad were present, but only a small anlagen of the presumptive metanephrogenic blastema was detectable (*H*) (arrow). Formation of tubules could not be seen in this mesenchyme. AD, adrenal gland; CG, cochlear ganglion; CO, cochlea; ED, endolymphatic duct; K, metanephric kidney; O, ovary; ON, optic nerve; OS, optic stalk; T, testis. (*A*, *B*, *G*, and *H*, bar = 200 μm; *C*–*F*, bar = 50 μm.)

markers or direct sequencing for a detailed analysis of the phenotypic effects in *Pax2*^{1Neu}/+ animals. In addition to the phenotypic effects on eye and kidney, some human *PAX2* heterozygotes suffer from mild sensorineural hearing loss (4). This correlates with the tissue-specific expression pattern of *Pax2*. An analysis of hearing ability in the mouse will require a systematic test protocol to determine if *Pax2* should be included in the list of mouse genes with hearing defects (25).

Crystal structure analysis of protein–DNA complexes showed that the paired domain contains two crucial domains involved in DNA binding: a type II β-turn (aa 13–16) and a helix–turn–helix motif (aa 20–60) (26). The *Pax2*^{1Neu} allele contains an insertion at codon 11 of the paired domain. The insertion results in a frameshift leading to a truncated protein in which the first 10 aa of the paired domain are normal, followed by 27 aa with only one match to the wild-type paired domain. A premature stop codon results in a deletion of the rest of the Pax2 protein. All DNA-binding domains required for specific base contacts are lost. Within the N-terminal β-sheet (aa 4–6 and 10–12), 2 aa remain that make contact to the DNA sugar phosphate backbone when in the context of the wild-type protein. For the mutant protein, they would not be expected to interact with a specific DNA sequence in the absence of the β-turn and the helix–turn–helix motif. We conclude that the truncated mutant protein is unable to recognize its normal target genes and nonfunctional.

Analysis of the phenotypic effects associated with *Pax2* −/− homozygotes is critical for an understanding of *Pax2* function in mammalian development. We are unaware of any human *PAX2* homozygous mutant cases. The mouse multilocus deletion *Krd* is homozygous lethal at the preimplantation stage, presumably due to the deletion of a linked gene or genes

essential for early development. Homozygotes for the mouse *Pax2* knockout mutation lack development of the kidney and genital tract (12). Our analyses extend the effects in *Pax2* −/− homozygotes to include defects in the development of the optic nerve, inner ear, and mid-hindbrain. These observations correlate well with the known tissue-specific expression pattern of *Pax2*.

The defects in the mid-hindbrain region are of special interest because several developmental control genes have been shown to play a role in establishing and patterning the mid-hindbrain region (for review, see ref. 21). Three *Pax* genes (*Pax2, Pax5, Pax8*) are expressed specifically in this region at early stages (3, 8–10, 21). Mouse mutants are known for *En1*, *En2*, *Wnt1*, *Pax2*, *Pax3*, *Pax5*, *Pax6*, and *Pax7,* but defects in development of the mid-hindbrain region have so far only been described for *En1*, *En2*, *Wnt1*, and *Pax5* (for review, see ref. 21) and *Pax2* (this study). *Pax5* homozygous mutant mice exhibit a reduction of the inferior colliculus and altered foliation pattern of the anterior cerebellum (27), whereas mutations in *Wnt1* and *En1* result in a much more pronounced deletion of the mid-hindbrain region (for review, see ref. 21). These findings suggest that loss of *Pax5* gene function is mostly compensated by other *Pax* genes (27). In this study, we show that a mutation in *Pax2* alone results in a deletion of the entire mid-hindbrain region that can already be observed at early stages of brain development. Thus, *Pax2* gene function is absolutely required for normal development of the mid-hindbrain region and cannot be compensated by the related *Pax5* and *Pax8* genes. This is consistent with the early expression of *Pax2* in the prospective mid-hindbrain region, preceding and encompassing the onset of *En1*, *En2*, *Wnt1*, *Pax5*, and *Pax8* genes (9, 10), and suggests that *Pax2* might regulate (directly or indirectly) *En1*, *En2*, and *Wnt1* gene expression. The deletions of the mid-hindbrain region that we observed in *Pax2* mutant embryos were very similar to those described for mutations of the *Wnt1* and *En1* genes (28, 29). Furthermore, two DNA-binding sites for *Pax2*, *Pax5*, and *Pax8* have been identified in the regulatory region of the *En2* gene (30) and, by inhibiting *Pax2* function after injection of antibodies in zebrafish embryos, *Wnt1* and *En2* expression was reduced leading to mid-hindbrain malformations (11). These results and our observations suggest that the regulatory interaction of genes involved in mid-hindbrain development in vertebrates is reminiscent of the situation in *Drosophila* where the pair-rule gene *paired* is required for activation of segment polarity genes, such as *wingless* and *engrailed* (for review, see ref. 21).

Several *Pax* genes have been described to play a role in human congenital diseases. The discovery of mouse mutants in the *Pax3* and *Pax6* genes has provided valuable animal systems with which the phenotypic alterations associated with the human aniridia/Peters anomaly and Waardenburg syndrome type I can be studied. Similarly, the present identification of a new *Pax2* allele in the mouse with the identical DNA alteration as in a human family with renal-coloboma syndrome should provide an ideal animal model for future studies on the congenital abnormalities associated with human *PAX2* mutations.

We thank T. Günther and Drs. R. Balling and C. Hoffmann for discussion of the manuscript and Utz Linzner, Institute of Pathology/Bioinformatics Workgroup, for the synthesis of the oligonucleotide primers. The Tskgel DNA-NPR-S ion exchange column for the HPLC purification of PCR products was kindly provided by TosoHaas, Stuttgart, Germany. This work was partially supported by grants from the Deutsche Forschungsgemeinschaft (K.S.), Sonderforschungsbereich 190 (W.W.), European Union (J.F.), and National Institutes of Health (J.F. and P.G.).

1. Strachan, T. & Read, A. P. (1994) *Curr. Opin. Genet. Dev.* **4,** 427–438.
2. Walther, C., Guenet, J.-L., Smion, D., Deutsch, U., Jostes, B., Goulding, M. D., Plachov, D., Balling, R. & Gruss, P. (1991) *Genomics* **11,** 424–434.
3. Wehr, R. & Gruss, P. (1996) *Int. J. Dev. Biol.* **40,** 369–377.
4. Sanyanusin, P., Schimmenti, L. A., McNoe, L. A., Ward, T. A., Pierpont, M. E. M., Sullivan, M. J., Dobyns, W. B. & Eccles, M. R. (1995) *Nat. Genet.* **9,** 358–364.
5. Sanyanusin, P., McNoe, L. A., Sullivan, M. J., Weaver, R. G. & Eccles, M. R. (1995) *Hum. Mol. Genet.* **4,** 2183–2184.
6. Nornes, H. O., Dressler, G. R., Knapik, E. W., Deutsch, U. & Gruss, P. (1990) *Development (Cambridge, U.K.)* **109,** 797–809.
7. Dressler, G. R., Deutsch, U., Chowdury, K., Nornes, H. O. & Gruss, P. (1990) *Development (Cambridge, U.K.)* **109,** 787–795.
8. Püschel, A. W., Westerfield, M. & Dressler, G. R. (1992) *Mech. Dev.* **38,** 197–208.
9. Rowitch, D. H. & McMahon, A. P. (1995) *Mech. Dev.* **52,** 3–8.
10. Kelly, G. M. & Moon, R. T. (1995) *Dev. Genet.* **17,** 129–140.
11. Krauss, S., Maden, M., Holdern, N. & Wilson, S. W. (1992) *Nature (London)* **360,** 87–89.
12. Torres, M., Goméz-Pardo, E., Dressler, G. R. & Gruss, P. (1995) *Development (Cambridge, U.K.)* **121,** 4057–4065.
13. Keller, S. A., Jones, J. M., Boyle, A., Barrow, L. L., Killen, P. D., Green, D. G., Kapousta, N. V., Hitchcock, P. F., Swank, R. T. & Meisler, M. H. (1994) *Genomics* **23,** 309–320.
14. Günther, T., Struwe, M., Aguzzi, A. & Schughart, K. (1994) *Development (Cambridge, U.K.)* **120,** 3119–3130.
15. Kaufman, M. H. (1992) *The Atlas of Mouse Development* (Academic, London).
16. Carter-Dawson, L., LeVail, M. & Sidman, R. (1978) *Invest. Ophtalmol. Visual Sci.* **17,** 489–498.
17. Maniatis, T., Fritsch, E. F. & Sambrook, J. (1989) *Molecular Cloning: A Laboratory Manual* (Cold Spring Harbor Lab. Press, Plainview, NY), 2nd Ed.
18. West, J. D., Peters, J. & Lyon, M. F. (1984) *Genet. Res.* **44,** 343–346.
19. Eccles, M. R., Wallis, L. J., Fidler, A. E., Spurr, N. K., Goodfellow, P. J. & Reeve, A. E. (1992) *Cell Growth Differ.* **3,** 279–289.
20. Weaver, R. G., Cashwell, L. F., Lorentz, W., Whiteman, D., Geisinger, K. R. & Ball, M. (1988) *Am. J. Med. Genet.* **29,** 597–605.
21. Joyner, A. L. (1996) *Trends Genet.* **12,** 15–20.
22. Carlson, B. M. (1988) *Patten's Foundations of Embryology* (McGraw–Hill, New York).
23. Silver, J. & Sapiro, J. (1981) *J. Comp. Neurol.* **202,** 521–538.
24. Horsburgh, G. M. & Sefton, J. (1986) *J. Comp. Neurol.* **243,** 547–560.
25. Steel, K. P. (1995) *Annu. Rev. Genet.* **29,** 675–701.
26. Xu, W., Rould, M. A., Jun, S., Desplan, C. & Pabo, C. O. (1995) *Cell* **80,** 639–650.
27. Urbanek, P., Wang, Z.-Q., Fetka, I., Wagner, E. & Busslinger, M. (1994) *Cell* **79,** 901–912.
28. McMahon, A. P. & Bradley, A. (1990) *Cell* **62,** 1073–1085.
29. Wurst, W., Auerbach, A. B. & Joyner, A. L. (1994) *Development (Cambridge, U.K.)* **120,** 2065–2075.
30. Song, D.-L., Chalepakis, G., Gruss, P. & Joyner, A. L. (1996) *Development (Cambridge, U.K.)* **122,** 627–635.